Investigation of Head Injury Mechanisms through Multivariate Finite Element Simulation

D. A. Jones[1,2], J. E. Urban[1,2], A. A. Weaver[1,2], and J. D. Stitzel[1,2]
[1] Wake Forest School of Medicine; [2] Virginia Tech-Wake Forest University Center for Injury Biomechanics

ABSTRACT

The purpose of this study was to evaluate the relationship between HIC and BrIC and injury metrics for real world intraparenchymal head injury in motor vehicle crashes (MVCs). Geometric and anatomically defined injury metrics were developed to study contusion, intraparenchymal hemorrhage, intraventricular hemorrhage, and DAI. The anatomically defined regions of interest included the fronto-temporal region, thalamus, corpus callosum, brain elements surrounding the ventricles, and a sphere of deep brain tissue. Geometrically defined regions of interest were developed based on impact location and were used to evaluate coup and contre-coup regions. 1,080 head impact simulations were conducted using the GHBMC 50th percentile finite element head and neck by varying impact direction, speed, location, and contact stiffness. Maximum principal strain, maximum shear strain, maximum pressure, and minimum pressure in each element was calculated for each simulation and correlations to HIC and BrIC were assessed. Positive pressures in the coup region were better correlated with HIC than BrIC (R^2 = 0.56 and R^2 = 0.35, respectively). Shear strain in the elements surrounding the ventricles was higher for off-axis loading compared to linear impacts ($p<0.001$). The average 50th percentile maximum shear strain in the corpus callosum (DAI) was better correlated with BrIC than HIC (R^2 = 0.82 and R^2 = 0.46, respectively) in soft and compliant impacts. Many of the strain measurements in the deep brain (Intraparenchymal hemorrhage, DAI) were unaffected by a change of impactor stiffness between compliant and hard. These data lend support to the continued discussion of efficacy of HIC and BrIC for the use of predicting head injury in MVCs.

INTRODUCTION

Over 1.7 million people sustain a Traumatic Brian Injury (TBI) annually in the United States, 52,000 of whom die. Nearly one third of TBIs resulting in death are the result of motor vehicle crashes (MVCs) or pedestrian impacts (Coronado, et al., 2011). To mitigate occupant injury in MVCs, vehicles are subject to government safety standards and are also given star ratings through the New Car Assessment Program (NCAP). These crash tests use anthropomorphic test devices (ATDs) to measure head linear acceleration and have the ability to measure rotational velocity. The resultant head linear acceleration is then used to compute the Head Injury Criterion (HIC). Supplementing the resultant linear acceleration of the head with measures of rotational velocity such as the Brain Injury Criterion (BrIC) has been proposed in

both Europe and the USA (Eppinger, et al., 1999; Takhounts, et al., 2003). A link between these two measures and real world injury has been minimal historically.

Brain injuries can be divided into multiple categories. Focal injuries consisting of hemorrhages and contusions are the source for the majority of intracranial legions. Example focal injuries include subdural hematoma, subarachnoid hemorrhage, contusion, intraparenchymal hemorrhage, and intraventricular hemorrhage. Converse to focal injuries are diffuse injuries, which form a spectrum ranging from concussion to the very severe diffuse axonal injury. The three most common injuries are intraventricular hemorrhage, subarachnoid hemorrhage, and subdural hematoma (Urban, et al., 2012; Urban, et al., 2015). These injuries can also be grouped based on their location within the head: intraparenchymal or extra-axial. Each of these injuries has an associated mortality and morbidity rate and can occur independently, or in combination. For this reason, it is important to study them on an individual basis.

Currently, the extent of measuring head injury risk in MVC safety testing is limited to linear acceleration measures such as HIC and peak acceleration (Hershman, 2001; IIHS, 2012; NHTSA, 1997). However, a long-standing hypothesis regarding head injury mechanisms requires the input of rotational kinematics to produce injury (Holbourn, 1943). Many research studies have demonstrated that the inclusion of rotational kinematics increases the incidence of certain head injuries compared to pure translation (Ommaya, et al., 1971). For this reason, Takhounts et al. developed a new head injury metric that captures peak head rotational velocities (BrIC) (Takhounts, et al., 2013).

The purpose of this study was to assess the correlation between ATD measurable values (HIC/BrIC) and intraparenchymal injury specific brain tissue injury metrics. These correlations were obtained through simulation and analysis of 1,080 head impacts with the Global Human Body Models Consortium (GHBMC) 50th percentile head and neck model (Gayzik, et al., 2011; Mao, et al., 2013). Head impact variables included speed, contact stiffness, direction, and location of impact. Geometric and anatomical regions of interest (ROIs) were developed for the analyses.

METHODS

Model Development

The head and neck were isolated from the GHBMC 50th percentile male finite element model (Gayzik, et al., 2011). The isolation was conducted at the T1 level, and all muscles that transcended the neck-thorax boundary were kept in the isolated model. Distal ends of the musculature were constrained to remain in place relative to T1 using *CONSTRAINED_EXTRA_NODES_SET. A 23 kg mass node was placed in the position of the thorax accelerometer in the full body model and constrained to T1 as demonstrated by the star and dashed line in Figure 1 (Pellman, et al., 2003). This mass was allowed to move in the horizontal plane, but was disallowed vertical (z-direction) movement (Comm, 2003).

Impact parameters

Location and direction. Videos and reports of crash test data from NHTSA as well as clinical head CT data from the CIREN database documenting soft tissue contusions/head contact were analyzed to determine possible locations of contact of the head during MVCs. Almost all locations on the head were potential impact locations so a set of 24 locations around one side of the GHBMC head were selected as "target locations". These target locations were selected by identifying nodes on the skin of the GHBMC M50 model at locations corresponding to Table 1 and shown in Figure 2.

Table 1: Number of impact locations at each elevation measuring from the head CG.

Elevation (degrees)	90	60	30	0	-30	-60
No. Locations	1	3	5	7	5	3

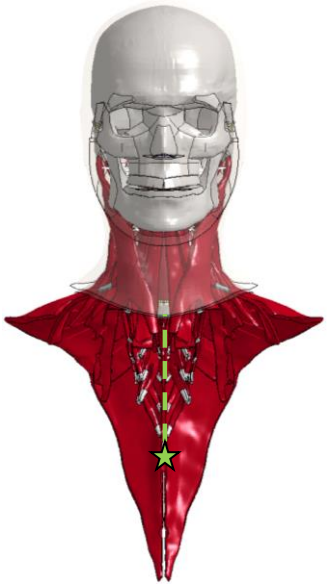

Figure 1: Isolated head and neck model from GHBMC 50th percentile male model. The star represents placement of the effective torso mass.

Local coordinate systems were created at each impact location to facilitate controlled impact vectors. The origin of each local coordinate system was the node defined as a "target location" with the x-axis point directly at the head CG. The z-axis and y-axis are roughly tangential to the surface of the head (Figure 3). At each impact location, the directionality of impact velocity was varied. One impact was directed in the direction of the CG of the head through the origin of the local coordinate system. Four other impacts were directed at the origin of the local coordinate system, but offset from the local x-axis by 45 degrees to include oblique impact scenarios (Figure 3). The off-axis loading is hereafter referred to as eccentric loading.

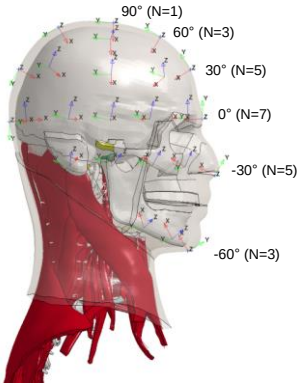

Figure 2: Local coordinate systems for impact simulations. Each local coordinate system is the target location for 5 impacts.

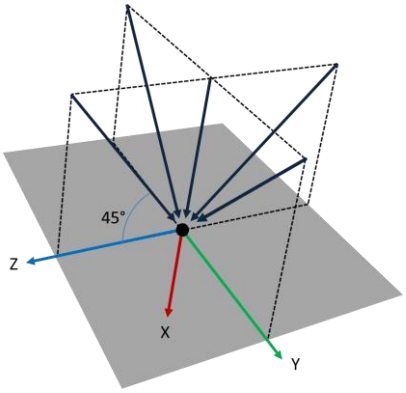

Figure 3: Directions of impact at each previously described local coordinate system. Five impact directions are prescribed per location.

Speed, stiffness, and geometry. Three impactor speeds were chosen after examining relative head velocity in 50 NHTSA crash tests with head impacts: 3, 5, and 10 m/s. In order to account for the various contact surfaces within a vehicle, the modulus of elasticity of the impactor was varied using three levels of stiffness while maintaining a mass of 12 kg and a diameter of 66 mm. The soft impactor, which was chosen to represent an airbag, was given a modulus of 165 kPa. The compliant material, which was supposed to approximate interior contacts such as an A-pillar, B-pillar, steering wheel, or dash, was assigned a modulus of 10 MPa. The hard material, chosen to resemble the steel of a pole or vehicle grills, was given an elastic modulus of 210 GPa.

Final test matrix. The final test matrix consisted of 24 different target impact locations with 5 impact vectors associated with each target. This yielded 120 impactor starting locations and vectors, 24 of which were classified as linear and 96 as eccentric. For each of these impact locations and vectors, both the stiffness and initial velocity of the impactor were varied. The resultant test matrix consisted of 1,080 simulations, targeting 24 different impact locations with 5 impact vectors with 3 impactor stiffnesses and 3 velocities (24x4x3x3=1080). 99.6% if the simulations terminated normally and were subsequently used for analysis.

Geometric and Anatomically Defined Regions of Interest

Geometric Cones. Twelve geometric ROIs were defined to quantitatively define coup and contre-coup regions. First, a vector was computed between the brain CG and the impact location. This is represented by the bold dashed line in Figure 4a. After this vector was established, a vector was calculated between each brain element and the head CG as well. Taking advantage of the mathematical cross-product, the angle between the element vector and the impact location vector was computed. Four specific ROIs were developed based on the following spatial distribution: <30°, <60°, >90°, and >120° from impact (Figure 4a). Following this step, the cones were divided into three equally spaced sections (Figure 4b). The outermost region (red) was referred to as "outer". The "intermediate" and "deep" sub-regions are shown in blue and green respectively. Combing angle and depth, specific ROIs could be narrowed down, (e.g., <30° outer, >120° intermediate, etc.).

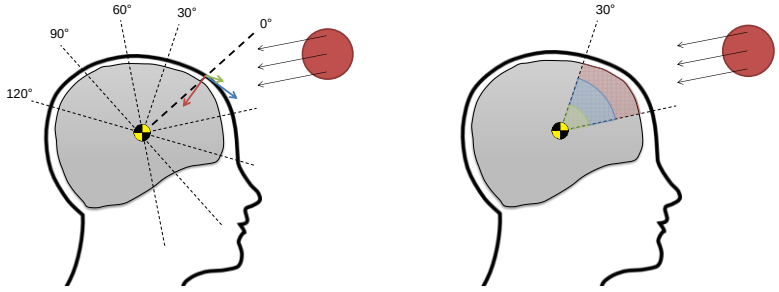

(a) (b)

Figure 4: Geometric region of interest diagram. Conical ROI angle measurements (a). Layered sub-regions: outer (red), intermediate (blue), deep (green) (b).

Anatomically defined ROIs. The frontal and temporal lobes are a common location of contusion (Ommaya, et al., 1971). Since the GHBMC does not natively define lobes, but instead has gray and white matter cerebrum parts, selecting a subset of these was important to capture

the frontal and temporal lobes. Each element of the Atlas-based Brain Model (ABM), developed by Miller et al., has a corresponding voxel in a label map of the brain (Miller, et al., 2016). Using these data, the ABM was scaled to the size of the GHBMC brain and aligned with the CG. Symmetric GHBMC elements touching either the frontal or temporal lobes of the ABM were selected to define the fronto-temporal ROI (Figure 5a).

Secondly, to assess intraventricular hemorrhage, which is caused by disruption of the ventricle walls, each element surrounding the ventricles was identified (Lindenberg, 1977). The ventricular wall ROI was developed by identifying any element sharing a node with the CSF elements that natively make up either the third or lateral ventricles in the GHBMC brain. This anatomical ROI is comprised of both white and gray matter (Figure 5b).

Finally, a sphere of deep brain tissue was defined to encapsulate the corpus callosum and neighboring structures in the deep brain of GHBMC. The center of the sphere is the brain CG and the volume extends radially to the anterior tip of the corpus callosum (Figure 5c). This ROI included the full corpus callosum, thalamus, midbrain, and basal ganglia as well as portions of the brainstem, cerebellum, and gray and white matter of the cerebrum.

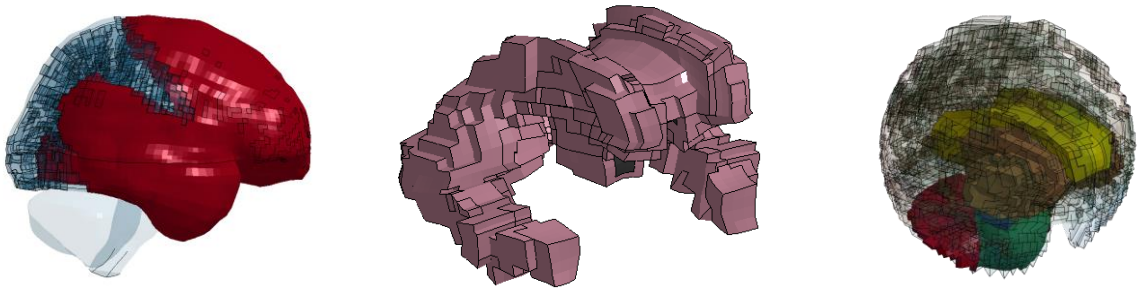

(a) (b) (c)

Figure 5: Anatomic regions of interest. Fronto-temporal ROI highlighted in red (a). Elements surrounding the ventricles in pink, with CSF in black (b). Deep brain sphere ROI (c). Corpus Callosum (yellow), basal ganglia (brown), cerebellum (red), brainstem (green), cerebrum (clear).

Injury Metrics

For all simulations, stress and strain data was recorded at 0.5 msec intervals for each element of the GHBMC brain matter. Peak values for maximum principal strain, maximum pressure, minimum pressure, and maximum shear strain were saved on an element by element basis for later use. Percentiles of the peak values in the ROIs were used for analysis. Statistical analyses were performed using two sample t-tests with significance levels of 0.05.

Contusion. Early research of contusion reported that the physical evidence of injury presented in both coup and contre-coup regions (Ommaya, et al., 1971). Some associate these finding with pressure gradients stemming from skull deformation, while others associate them with strain (Gurdjian, et al., 1944; Nusholtz, et al., 1995; Shatsky, et al., 1974). Regardless of mechanism, a common pattern of occurrence in the frontal and temporal lobes was observed (Ommaya, et al., 1971). Therefore, a fronto-temporal ROI was chosen for evaluation of contusion as well as the <60° and >120° outer cone ROIs. Pressure distribution was analyzed using the geometric ROIs, while maximum principal strains in the fronto-temporal ROI were analyzed. For both pressures and strains, the 90^{th} percentile of the maximum values in the ROI were used for comparison to HIC and BrIC.

Intraparenchymal hemorrhage. Intraparenchymal hemorrhage, the injury defined by bleeding anywhere within the brain parenchyma, often occurs in the deep portions of the brain (Gennarelli, et al., 1972). Moreover, thalamic hemorrhage constitutes between 20 and 35% of all cerebral hemorrhages (Kwak, et al., 1983). Therefore, maximum principal strain was gathered in both the deep brain sphere ROI and the thalamus. Since bleeds require only one isolated source of damage, the 90^{th} percentile of the maximum principal strain in the region was computed and used for comparison to ATD measurable metrics.

Intraventricular hemorrhage. Intraventricular hemorrhage is defined as bleeding into the brain's ventricular system and is likely due to damage to the wall of the lateral or third ventricle, the ventral portion of the corpus callosum, the fornicles, or the choroid plexus (Lindenberg, 1977). For this reason the injury was assessed by computing the 90^{th} percentile of the maximum shear stress in the ROI defined by the elements surrounding the ventricles (Figure 5b).

Diffuse axonal injury. Diffuse axonal injury (DAI) is by nature an injury that is often dispersed throughout the brain. Clinically, it is often seen at the junction of the white and gray matter (subcortical gray matter) as well as deep within the splenium of the corpus callosum and is thought to be caused by shearing of the axons (Adams, et al., 1977). Thus, instead of identifying the highest strains in the ROIs, 50^{th} percentile maximum principal strains were collected. Both the corpus callosum, defined as an independent part in the GHBMC model, and the previously described deep brain sphere were analyzed separately. For reference, it has been reported that when 54% of the brain exceeds a threshold of 25% strain, there is an associated 50% risk of DAI (Takhounts, et al., 2008).

RESULTS

Contusion

For hard impacts through the CG, peak pressure in the coup (<60° outer) and contre-coup (>120° outer) ROIs, the peak pressure in each element was gathered and the 90^{th} percentile stored. Figure 6 shows that the 90^{th} percentile peak pressure is significantly higher in the coup region compared to the contre-coup region in hard linear impacts regardless of speed. Positive pressures in the coup region were better correlated with HIC than BrIC ($R^2 = 0.56$ and $R^2 = 0.35$, respectively).

In the contre-coup region, it is known that negative pressures develop. The lowest 10% of the minimum pressures (10^{th} percentile minimum pressure) in each ROI are presented in Figure 7. The findings demonstrate that on average the contre-coup region experiences lower pressures than the coup region in all hard impacts. Negative pressures in the coup region were better correlated with HIC than BrIC ($R^2 = 0.39$ and $R^2 = 0.21$, respectively).

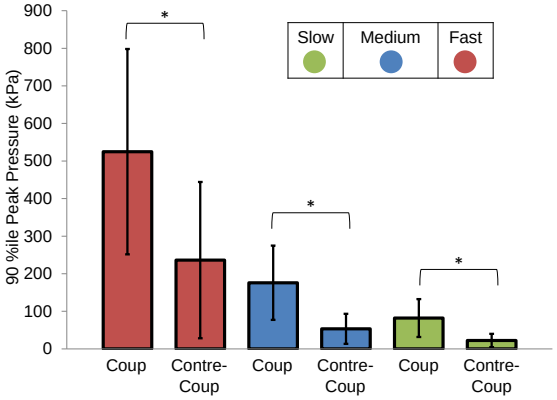

Figure 6: 90th percentile of the peak pressure in <60° outer (coup) and >120° outer (contre-coup) ROIs for linear, hard impact simulations.

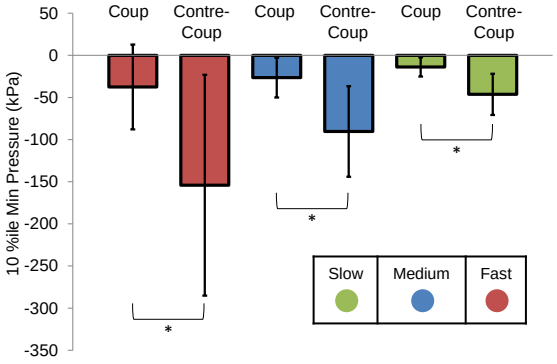

Figure 7: 10th percentile of the minimum pressure in <60° outer (coup) and >120° outer (contre-coup) ROIs for linear, hard impact simulations.

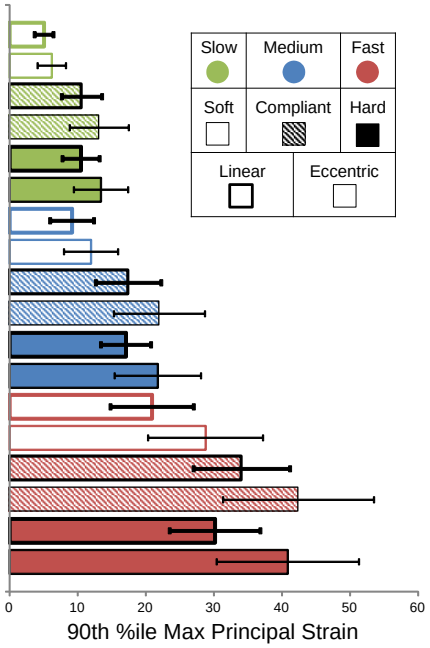

Figure 8: Mean and standard deviation of 90th percentile maximum principal strains for the fronto-temporal lobe regions.

Results from the 90th percentile maximum principal strain in the fronto-temporal ROI were compared between impact conditions (Figure 8). For all speeds, the mean 90th percentile strain was higher in eccentric loading compared to linear impacts. Next, this strain distribution was plotted against HIC and BrIC. Since, contusions are frequently associated with skull fracture (60-80%) and the hard impact simulations produced the most skull fractures, only hard impacts are shown (Figure 9) (Cooper, 1982). Linear regression analysis shows that 90th percentile of maximum principal strains in the fronto-temporal ROI has a statistically significant correlation with both HIC and BrIC ($p<0.0001$), but the coefficient of determination is much higher for BrIC ($R^2=0.918$ vs $R^2=0.347$). Thus, BrIC is a better correlate with fronto-temporal strain in all hard impacts.

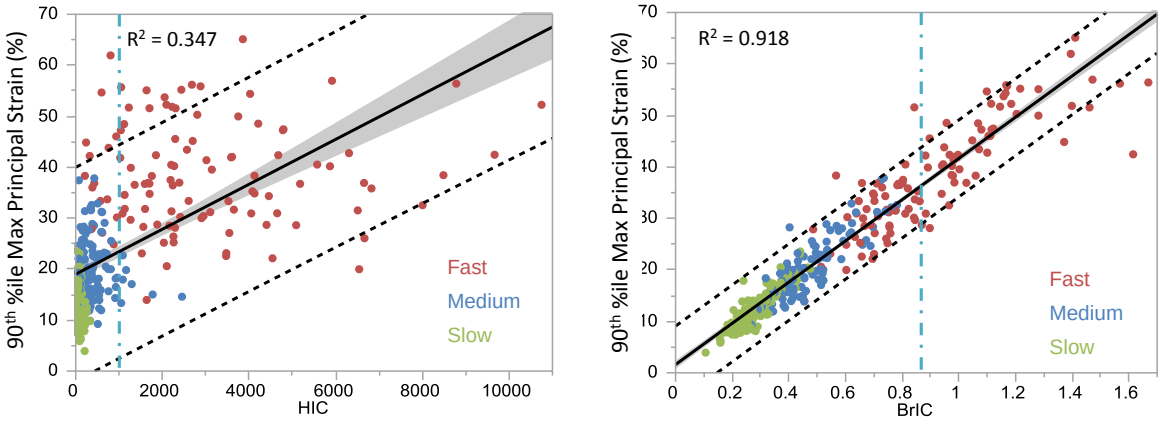

Figure 9: 90th percentile of the maximum principal strain in the fronto-temporal ROI from hard impacts not excluding skull fracture. Vertical blue dashed lines represent 50% risk of AIS 3+ injury. Gray shading represents 95 % confidence intervals of the fit. Gray dashed lines represent 95% confidence intervals on individual values.

Intraparenchymal Hemorrhage

Intraparenchymal hemorrhage was evaluated by computing the strain in the deep brain sphere and the thalamus (Figure 10). There is a statistically significant difference in the means of the 90th percentile maximum principal strains when comparing linear and eccentric loading simulations for all hard and compliant impacts. Statistical significance was reached for soft impacts only in the fast speed for the thalamus, and in both fast and medium speed for the deep brain sphere.

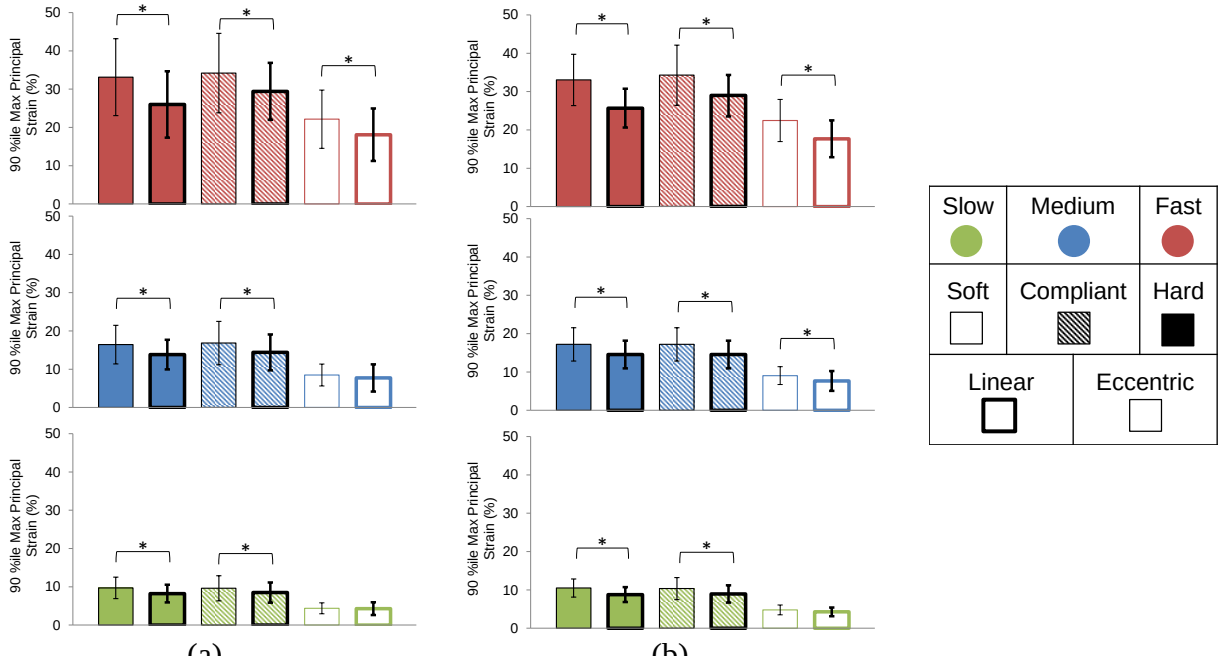

(a) (b)

Figure 10: 90th percentile maximum principal strain in the thalamus (a) and the deep brain sphere (b).

There was little difference between the strain distributions between hard and compliant impacts for both the thalamus and the deep brain sphere. However, soft impacts resulted in lower 90th percentile maximum principal strains than either compliant or hard impacts. Overall, the 90th percentile maximum principal strains were similar between the deep brain sphere and the thalamus.

Intraventricular Hemorrhage

The elements surrounding the ventricles and the CSF in the GHBMC brain were analyzed for high shear strains. Ommaya et al., recognized that soft impacts that extended the duration of the acceleration pulse were needed to produce damage to deep structures (Ommaya, 1985). Therefore, only compliant and soft impacts were evaluated for association with IVH. The mean 90th percentile maximum shear strain was significantly higher for eccentric impacts compared to the matched condition linear impacts (Figure 11).

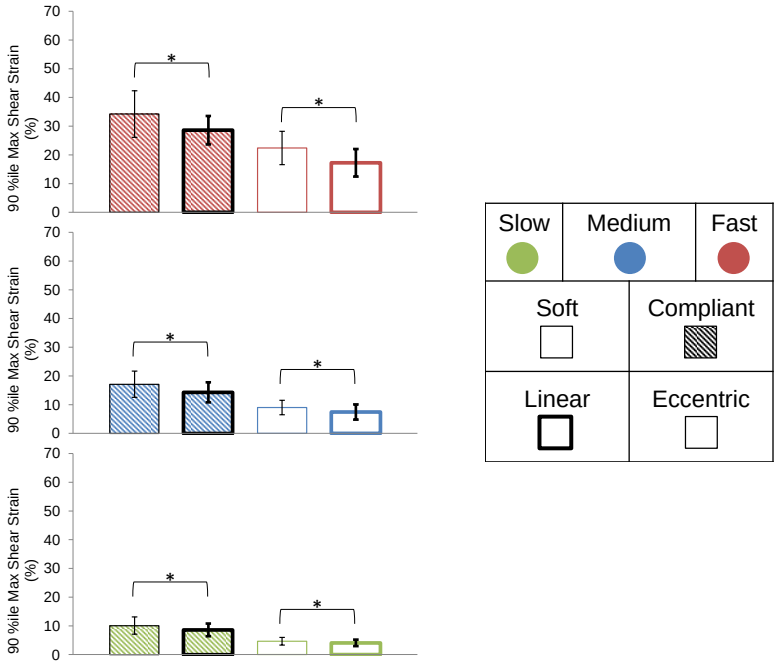

Figure 11: 90th percentile maximum shear strain in the elements surrounding the ventricles for soft and compliant impacts. Skull fracture cases included. Statistical significance was found between linear and eccentric loading at every speed and impactor stiffness.

To assess the effects of linear and rotational kinematics on shear strains in this ROI, the 90th percentile maximum shear strain was regressed against HIC and BrIC (Figure 12). In both compliant and soft impacts, BrIC had a higher R^2 value compared to HIC. High shear strains (>30%) were present even in soft contacts.

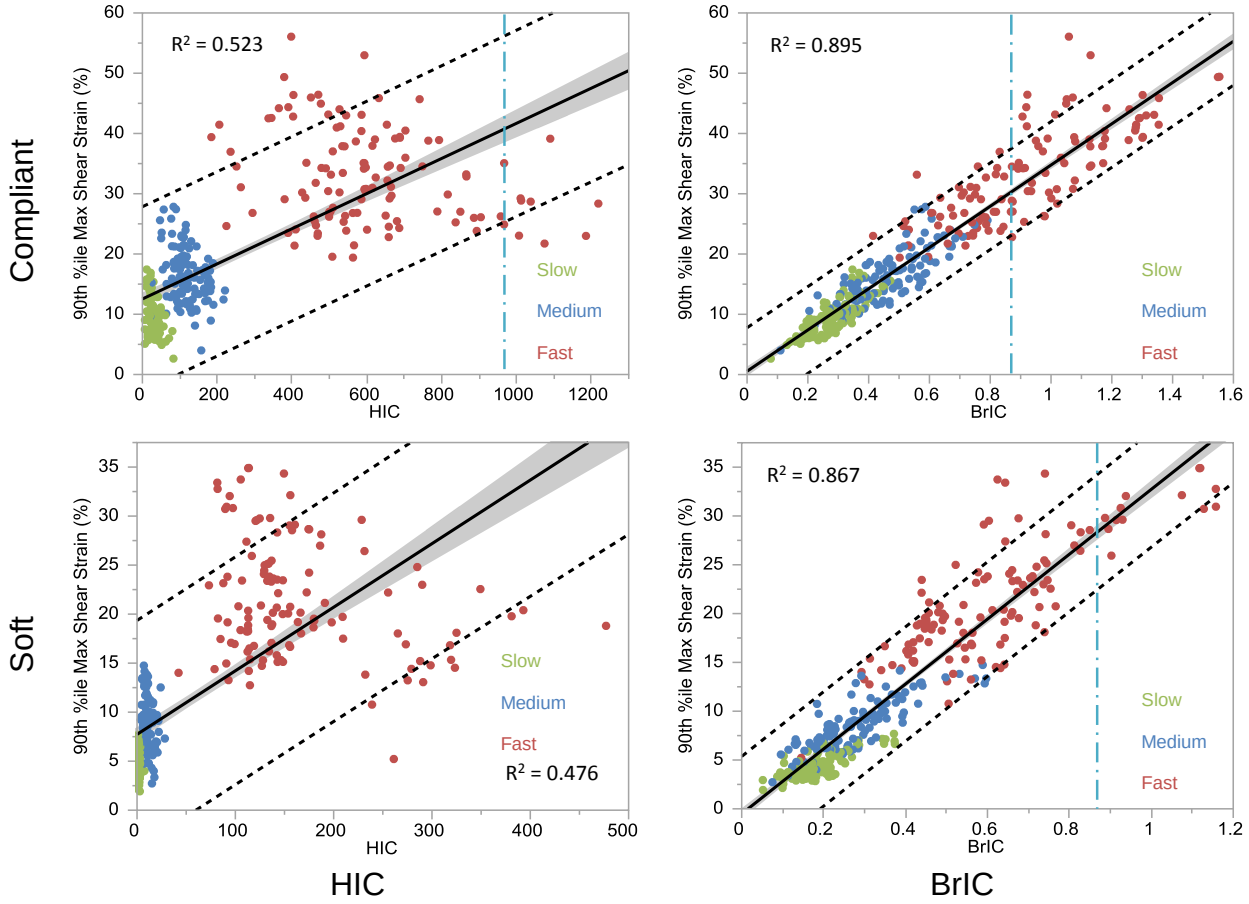

Figure 12: 90th percentile maximum shear strain in the elements surrounding the ventricles. Soft and compliant impacts, including cases with skull fracture. Vertical blue dashed lines represent 50% risk of AIS 3+ injury. Gray shading represents 95 % confidence intervals of the fit. Gray dashed lines represent 95% confidence intervals on individual values.

Diffuse Axonal Injury

The 50th percentile maximum shear strain the deep brain sphere was regressed against HIC and BrIC for compliant and soft impacts (Figure 13). Though BrIC demonstrated better correlation (R^2 = 0.89 and R^2 = 0.53, respectively), 50th percentile maximum shear strain in the deep brain increased with increasing HIC and BrIC. Similar results were found for the corpus callosum (R^2 = 0.82 and R^2 = 0.46, respectively).

To compare the mean 50th percentile maximum shear strain in the deep tissues, linear and eccentric loads were plotted next to each other for all impact speeds and stiffnesses (Figure 14). Statistical analysis shows that eccentric loading consistently produced higher strains than linear loading across all levels in both the corpus callosum and the deep brain sphere. It should be noted that strains in just the corpus callosum were higher than in the deep brain sphere. Additionally, the change from hard impactor to compliant impactor did not significantly affect strain distributions.

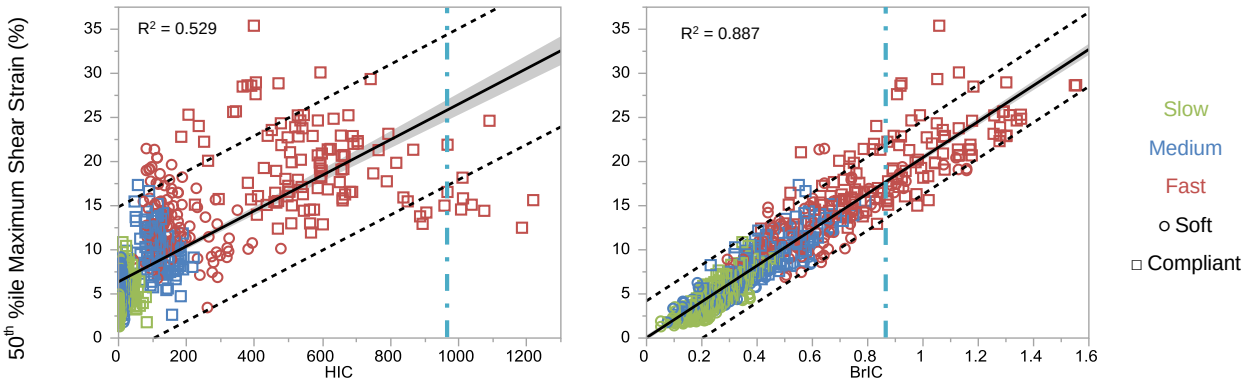

Figure 13: 50th percentile maximum shear strain in the deep brain sphere ROI. Vertical blue dashed lines represent 50% risk of AIS 3+ injury. Gray shading represents 95% confidence intervals of the fit. Gray dashed lines represent 95% confidence intervals on individual values.

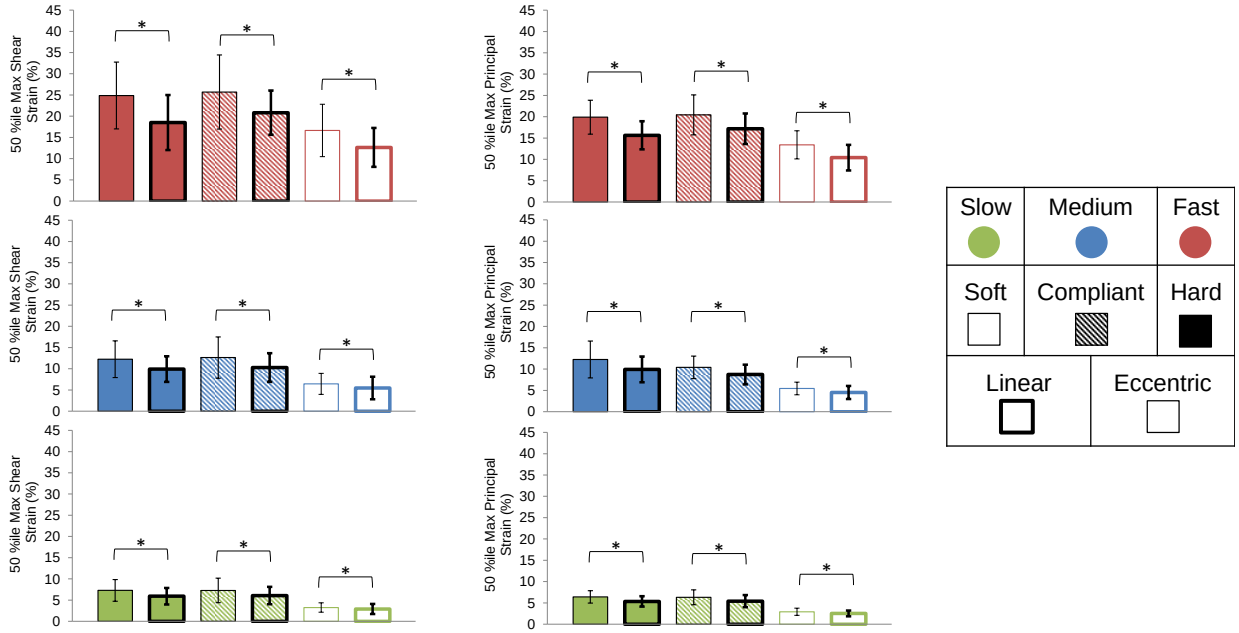

(a) (b)

Figure 14: 50th percentile maximum principal strain in the corpus callosum (a) and the deep brain sphere (b).

DISCUSSION

Contusion

The Head Injury Criterion was a better predictor of positive pressure in the coup region and negative pressure in the contre-coup region compared to BrIC. Magnitude of pressure measurements decreased with decreasing impactor velocity for hard impacts. Though pressure correlated well with HIC, strain in the fronto-temporal lobes was consistently higher for

eccentric loading compared to linear impacts. This manifests itself in the significantly stronger correlation with BrIC than HIC.

Intraparenchymal Hemorrhage

There was little difference between the maximum principal strain distribution between the thalamus, and the deep brain sphere. Though eccentric loading produced higher strains in these deep tissue regions, the strains remained similar given a hard or compliant impactor. Since many of the hard impacts in the fast regime produced skull fracture, this suggests that skull fracture likely does not affect strain in the deep tissues.

Intraventricular Hemorrhage

Shear strain along the walls of the ventricles was positively correlated with both HIC and BrIC, however BrIC achieved a stronger correlation. For both soft and compliant impacts, the correlation between BrIC and 90th percentile maximum shear strain in the ventricles was above R^2=0.86.

Diffuse Axonal Injury

Finally, DAI measures, namely 50^{th} percentile maximum shear strain, was higher in the corpus callosum than in the deep brain sphere ROI. This aligns with the classical location of DAI. The mean 50^{th} percentile shear strain in these ROIs was slightly higher for compliant impacts compared to hard impacts. Both HIC and BrIC correlated well with shear strain in the deep brain sphere ($R^2 > 0.529$).

CONCLUSIONS

1,080 impact simulations were conducted with the GHBMC 50^{th} percentile head and neck model. Geometric and anatomically defined regions of interest were developed on a per-injury basis for evaluation of brain tissue metrics including pressure and strain. These ROI based injury metrics were correlated with HIC and BrIC and were compared against impact type.

With the continued discussion of the efficacy of HIC and BrIC for the use of predicting head injury in MVCs, this data presents evidence for the continued consideration of both. HIC was a better correlator with both positive and negative pressure in the coup and contre-coup regions respectively, while BrIC was better correlated with strain regardless of the region or impact stiffness.

ACKNOWLEDGEMENTS

Views expressed are those of the authors and do not represent the views of any sponsors. Funding for this project was provided by the National Highway Traffic Safety Administration under Cooperative Agreement Number DTNH22-10-H-00294. The M50-O v. 4.1 model was developed as part of the Global Human Body Models Consortium project. The authors gratefully acknowledge the contributions of the Full Body Models COE at Wake Forest

University (PIs, FS Gayzik, JD Stitzel), the Head COE at Wayne State University (PI, L Zhang) and the Neck COE at University of Waterloo (PI, DS Cronin). The authors would like to thank Casey Costa for help in development of the boundary conditions for the simulations.

REFERENCES

Adams H, Mitchell DE, Graham D, Doyle D. Diffuse brain damage of immediate impact type. Its relationship to'primary brain-stem damage'in head injury. *Brain: a journal of neurology.* 1977;100(3):489-502.

Comm STIS. *Instrumentation for impact test-part 1-electronic instrumentation (j211/1)*: Technical report, SAE;2003.

Cooper PR. Post-Traumatic Intracrianial Mass Lesions. In: Cooper PR, ed. *Head Injury.* Baltimore/London: Williams and Wilkins; 1982.

Coronado VG, Xu L, Basavaraju SV, et al. Surveillance for traumatic brain injury-related deaths--United States, 1997-2007. *MMWR Surveill Summ.* May 6 2011;60(5):1-32.

Eppinger R, Sun E, Bandak F, et al. Development of improved injury criteria for the assessment of advanced automotive restraint systems–II. 1999.

Gayzik FS, Moreno DP, Geer CP, Wuertzer SD, Martin RS, Stitzel JD. Development of a full body CAD dataset for computational modeling: a multi-modality approach. *Ann Biomed Eng.* Oct 2011;39(10):2568-2583.

Gennarelli TA, Thibault L, Ommaya A. Pathophysiologic responses to rotational and translational accelerations of the head. Paper presented at: Proceedings: Stapp Car Crash Conference1972.

Gurdjian E, Lissner H. Mechanism of Head Injury as Studied by the Cathode Ray Oscilloscope* Preliminary Report. *Journal of Neurosurgery.* 1944;1(6):393-399.

Hershman LL. The US new car assessment program (NCAP): Past, present and future. Paper presented at: International Technical Conference on the Enhanced Safety of Vehicles2001.

Holbourn A. Mechanics of head injuries. *The Lancet.* 1943;242(6267):438-441.

IIHS. *Small Overlap Frontal Crashworthiness Evaluation Rating Protocol.* Arlington, VA2012.

Kwak R, Kadoya S, Suzuki T. Factors affecting the prognosis in thalamic hemorrhage. *Stroke.* 1983;14(4):493-500.

Lindenberg R. Pathology of craniocerebral injuries. In: Newton TH, Potts DG, eds. *Radiology of the skull and brain: Anatomy and Pathology.* Vol 3: C.V. Mosby Co.; 1977.

Mao H, Zhang L, Jiang B, et al. Development of a finite element human head model partially validated with thirty five experimental cases. *J Biomech Eng.* Nov 2013;135(11):111002.

Miller LE, Urban JE, Stitzel JD. Development and validation of an atlas-based finite element brain model. *Biomech Model Mechanobiol.* Jan 13 2016.

NHTSA. *Final Regulatory Evaluation, Actions to Reduce the Adverse Effects of Air Bags - FMVSS No. 208 DEPOWERING*1997.

Nusholtz GS, Wylie B, Glascoe LG. Cavitation/boundary effects in a simple head impact model. *Aviation, space, and environmental medicine.* 1995;66(7):661-667.

Ommaya AK. Biomechanics of head injury: experimental aspects. *The biomechanics of trauma.* 1985;13:245-269.

Ommaya AK, Grubb RL, Jr., Naumann RA. Coup and contre-coup injury: observations on the mechanics of visible brain injuries in the rhesus monkey. *J Neurosurg.* Nov 1971;35(5):503-516.

Ommaya AK, Hirsch AE. Tolerances for cerebral concussion from head impact and whiplash in primates. *J Biomech.* Jan 1971;4(1):13-21.

Pellman EJ, Viano DC, Tucker AM, Casson IR, Waeckerle JF. Concussion in professional football: reconstruction of game impacts and injuries. *Neurosurgery.* Oct 2003;53(4):799-812; discussion 812-794.

Shatsky SA, Alter WA, Evans DE, Armbrustmacher VW, Clark G, Earle KM. Traumatic distortions of the primate head and chest: correlation of biomechanical, radiological and pathological data. Paper presented at: Proceedings: Stapp Car Crash Conference1974.

Takhounts EG, Craig MJ, Moorhouse K, McFadden J, Hasija V. Development of brain injury criteria (BrIC). *Stapp Car Crash J.* Nov 2013;57:243-266.

Takhounts EG, Eppinger RH, Campbell JQ, Tannous RE, Power ED, Shook LS. On the Development of the SIMon Finite Element Head Model. *Stapp Car Crash J.* Oct 2003;47:107-133.

Takhounts EG, Ridella SA, Hasija V, et al. Investigation of traumatic brain injuries using the next generation of simulated injury monitor (SIMon) finite element head model. *Stapp Car Crash J.* Nov 2008;52:1-31.

Urban JE, Whitlow CT, Edgerton CA, Powers AK, Maldjian JA, Stitzel JD. Motor vehicle crash-related subdural hematoma from real-world head impact data. *J Neurotrauma.* Dec 10 2012;29(18):2774-2781.

Urban JE, Whitlow CT, Stitzel JD. Investigation of Intraventricular Hemorrhage Volume in Motor Vehicle Crash Occupants. *Trauma cases Rev.* 2015;1(4).